Gas-Particle Flow in a Duct of Arbitrary Inclination with Particle-Particle Interactions

R. Ocone, S. Sundaresan, and R. Jackson
Princeton University, Princeton, NJ 08544

Earlier work of Sinclair and Jackson on the flow of gas-particle suspensions in vertical pipes is extended to the case of ducts of arbitrary inclination. As a result of the compaction due to gravity, it is necessary to take into account forces transmitted between particles at points of sustained, rolling and sliding contact, and a simple frictional model of this contribution to the stress is introduced. The resulting theory is shown to predict fully developed flows with the qualitative features to be expected, even in horizontal ducts. The effects of flow rates, duct inclination, and duct width on the solution are explored.

Introduction

In an earlier article, Sinclair and Jackson (1989) analyzed the laminar flow of a gas-particle suspension in a vertical tube, taking into account the interactions among the particles by mutual collisions. The solutions, which were obtained for fully developed cocurrent upflow, cocurrent downflow, and countercurrent flow, exhibited a surprising variety of structure, with the possibility of multiple solutions that seemed to correspond to observed phenomena, such as choking and flooding. Furthermore, the well known tendency to nonuniform spatial distribution of the particles, with a high concentration near the tube wall, was predicted well, though the detailed form of the particle concentration profile depended quite strongly on the assumed values of parameters such as coefficients of restitution.

Though many flows of practical interest are expected to be turbulent, before attempting to model these it is worthwhile to extend the investigation of laminar flows to the case of ducts inclined to the vertical where the cross-sectional distribution of the particles is influenced by gravity, which tends to move them toward the lower part of the duct. Nonvertical ducts are important, for example, in pneumatic transport where particles may have to be moved substantial distances through horizontal or gently inclined ducts, and in standpipes used to transport particles against an adverse gas pressure gradient with the help of gravity. Though these work best when vertical, for practical reasons they must often be inclined. When the inclination to the vertical is large, gravitational sedimentation may generate very high concentrations of particles near the lower surface of the duct; for example, in horizontal pipes particles may "settle out" in a dense layer, which is dragged slowly along by the fast moving, but more dilute, suspension above it. In such a layer, we would expect the interaction between the particles to result from forces exerted at points of sustained rolling and sliding contact, rather than brief "collisions" of the sort envisaged by Sinclair and Jackson. To treat this type of situation, the equations used by Sinclair and Jackson must, therefore, be generalized by including additional terms to represent stress transmission in the particle assembly by this mechanism. Unfortunately, there is no general theory of stress in moving assemblies of particles interacting by forces transmitted at points of solid-solid contact, though there are treatments based on the kinetic theory of dense gases (for a recent review of these, see Campbell, 1990) for the case where contacts take the form of brief collisions and quite different, essentially empirical treatments of the opposite limiting case where each particle is in sliding and rolling contact with several neighbors. Theories for the latter case have their origin in soil mechanics, and some of the simpler ideas have been reviewed by Jackson (1983). When it is necessary to treat situations between the two extremes, all that is presently available in an additivity hypothesis of Savage (1982), who suggested that the contributions to the stress from the two extreme mechanisms should be calculated, each as though it acted alone, then the two should simply be added to give the total stress. This idea has been used by Johnson and Jackson (1987) and Johnson et al. (1990) to treat the motion of a dry granular material sheared between horizontal plates or in motion under gravity down an inclined plane, respectively, and the results have been found to model the observed behavior quite well over a wide range of conditions. It will, therefore, be used here to treat suspension flows.

Formulation of the Problem

The approach resembles closely that of Sinclair and Jackson (1989). In the present case, the physical model is generalized by including the "frictional" contributions to particle phase stress discussed above, and the geometric configuration is generalized by allowing the flow duct to assume an arbitrary angle of inclination. In Sinclair and Jackson's treatment the vertical duct was taken to be a tube of uniform circular cross section. Then, in fully developed flow, only the radial coordinate appears nontrivially in the equations, which therefore reduce to ordinary differential equations. When the duct is inclined to the vertical, this symmetry is broken by the gravitational force, and partial differential equations need to be solved. To avoid this, in the present work the tube is replaced by a duct formed between two infinite, parallel plates separated by a distance H, as shown in Figure 1. Cartesian coordinates are taken, with the origin in the lower plate, the y axis perpendicular to the line of flow, and the x axis directed up the slope, as indicated. Then, the equations to be solved take the following form for fully developed flow:

$$\frac{\partial}{\partial y}\left[\mu_{eg}(\nu)\frac{\partial u}{\partial y}\right]-\beta(\nu)(u-v)-\frac{\partial p}{\partial x}=0 \tag{1}$$

representing the component of momentum balance in the x direction for the gas:

$$-\frac{\partial \sigma_{xy}}{\partial y}+\beta(\nu)(u-v)-\rho_p \nu g \sin\theta=0 \tag{2}$$

representing the component of momentum balance in the x direction for the particles:

$$\frac{\partial \sigma_{yy}}{\partial y}+\rho_p \nu g \cos\theta=0 \tag{3}$$

representing the component of momentum balance in the y direction for the particles, and

$$\frac{\partial q_{PT}}{\partial y}+\sigma^c_{xy}\frac{\partial v}{\partial y}+I=0 \tag{4}$$

representing a balance of the "pseudothermal" energy of fluctuations in particle velocity resulting from collisions. In these equations,

- u, v = local average values of x components of velocity for gas and particles, respectively
- p = pressure of the gas
- σ_{ij} = components of the stress tensor of the particle phase, defined in the compressive sense
- σ^c_{ij} = components of the kinetic-collisional (see below) contribution to the particle phase stress tensor
- ν = volume fraction of space occupied by the particles
- ρ_p = density of the solid material from which the particles are formed
- g = gravitational acceleration
- μ_{eg} = effective viscosity of the gas in the presence of the particles
- q_{PT} = y-component of the pseudothermal energy flux
- I = dissipation rate of pseudothermal energy by inelastic collisions, per unit total volume

The term $\beta(\nu)(u-v)$ appearing in Eqs. 1 and 2 represents the drag force per unit total volume exerted between the two phases as a result of their relative motion, and a form for the drag coefficient β is based on the Richardson-Zaki (1954) equation:

$$\beta(\nu)=\frac{\rho_p \nu g}{v_t(1-\nu)^n} \tag{5}$$

where v_t is the terminal velocity of fall of an isolated particle under gravity, and the exponent n depends on the particle Reynolds number at this velocity.

To close this set of equations we use expressions for μ_{eg} and I of the same form as those adopted by Sinclair and Jackson (1989):

$$\mu_{eg}(\nu)=\mu_g(1+2.5\nu+7.6\nu^2)(1-\nu/\nu_0) \tag{6}$$

$$I=\frac{48}{\pi^{1/2}}\eta(1-\eta)\frac{\rho_p \nu^2}{d}g_0 T^{3/2} \tag{7}$$

where T is the particle temperature, related to the kinetic energy of random motion by $T=c^2/3$ where c^2 is the mean square velocity fluctuation, d is the particle diameter, ν_0 is the volume fraction solids at random close packing, η represents $(1+e_p)/2$, where e_p is the coefficient of restitution for collisions between particles, and $g_0=1/[1-(\nu/\nu_0)^{1/3}]$.

The closure for the stress in the particle phase differs from that used by Sinclair and Jackson as we write:

$$\sigma=\sigma^c+\sigma^f \tag{8}$$

where the terms on the righthand side represent the "kinetic-collisional" and the "frictional" contributions to the particle phase stress, respectively. As in the earlier work, a form for σ^c proposed by Lun et al. (1984) is used:

$$\sigma^c=[\rho_p \nu T(1+4\eta\nu g_0)-\eta\mu_b\nabla\cdot\mathbf{v}]I$$
$$-\left\{\frac{2\mu_i}{g_0}\left(1+\frac{8}{5}\eta\nu g_0\right)\left[1+\frac{8}{5}\eta(3\eta-2)\nu g_0\right]+\frac{6}{5}\mu_b\eta\right\}S \tag{9}$$

where I denotes the unit tensor, S is the deviatoric part of the

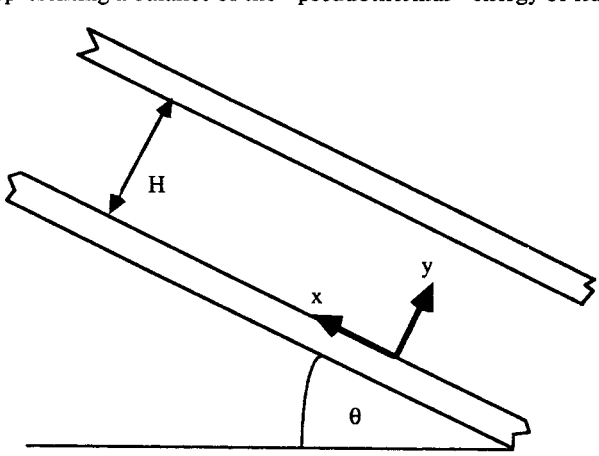

Figure 1. The system.

stress tensor for the particle phase:

$$S = 1/2[\nabla \mathbf{v} + (\nabla \mathbf{v})^T] - 1/3(\nabla \cdot \mathbf{v})I$$

and

$$\mu = \frac{5m(T/\pi)^{1/2}}{16d^2} \quad \mu_b = \frac{256\mu\nu^2 g_0}{5\pi} \quad \mu_i = \frac{\mu}{\eta(2-\eta)}$$

where m is the mass of one particle. The literature of soil mechanics contains a variety of expressions which could be used for σ^f, but fortunately, for the case of plane shear, they all reduce to a common form. The shear and normal components of stress are related by:

$$|\sigma^f_{xy}| = \sigma^f_{yy} \sin \phi \tag{10}$$

where ϕ is an angle of friction characteristic of the particles, and the normal component of stress depends on the concentration of the particles, diverging as this approaches random close packing. For this, we adopt a functional form used previously by Johnson et al. (1990):

$$\sigma^f_{yy} = Fr \frac{(\nu - \nu_m)^{n_1}}{(\nu_0 - \nu)^p} \quad \text{for} \quad \nu > \nu_m$$

$$= 0 \quad \text{for} \quad \nu < \nu_m \tag{11}$$

where Fr, p, and n_1 are empirical constants.

Finally, the pseudothermal energy flux is written in the form proposed by Lun et al. (1984):

$$\mathbf{q}_{PT} = -\frac{\lambda_i}{g_0}\left\{\left(1+\frac{12}{5}\eta\nu g_0\right)\left[1+\frac{12}{5}\eta^2(4\eta-3)\nu g_0\right] + \frac{64}{25\pi}(41-33\eta)(\eta\nu g_0)^2\right\}\nabla T$$

$$-\frac{\lambda_i}{g_0}\left(1+\frac{12}{5}\eta\nu g_0\right)\frac{12}{5}\eta(2\eta-1)(\eta-1)\frac{d}{d\nu}(\nu^2 g_0)\frac{T}{\nu}\nabla\nu \tag{12}$$

where

$$\lambda_i = \frac{8\lambda}{\eta(41-33\eta)} \quad \text{with} \quad \lambda = \frac{75m(T/\pi)^{1/2}}{64d^2}$$

Jenkins (1987) has pointed out that η may be replaced by unity everywhere in the above expressions (except in Eq. 7 for the dissipation rate, where $1-\eta$ is the leading order term) without significant change in the results. This simplifies the algebra somewhat and may also ensure that the order of approximation for $1-\eta$ which is assumed to be small, corresponding to almost elastic collisions, is consistent in all the expressions.

To complete the formulation of the problem, boundary conditions must be specified at the walls of the duct. The first of these is found by equating the transfer rate of axial momentum from the particles to the wall and the limit of the tangential stress in the particle assembly on approaching the wall. In this way, Johnson and Jackson (1987) found:

$$\frac{\mathbf{n}\cdot\sigma\cdot\mathbf{v}}{|\mathbf{v}|} + \sigma^f_{yy}\tan\delta' + \frac{\phi'\sqrt{3}\,\pi\rho_p\nu T^{1/2}|\mathbf{v}|}{6\nu_0[1-(\nu/\nu_0)^{1/3}]} = 0 \tag{13}$$

where $\mathbf{n}$ denotes the unit normal drawn from the wall into the flowing suspension, δ' is the angle of friction for particles sliding over the wall, and ϕ' is a specularity factor which varies between zero, when collisions between particles and the wall are perfectly specular, and unity when they are completely diffuse. Similarly, by performing a pseudothermal energy balance on a thin control region enclosing the wall, Johnson and Jackson derived a boundary condition for the pseudothermal energy flux which can be written in the form

$$\mathbf{n}\cdot\mathbf{q}_{PT} = \frac{\pi\rho_p\nu\sqrt{3T}}{6\nu_0[1-(\nu/\nu_0)^{1/3}]}\left[\phi'|\mathbf{v}|^2 - \frac{3T}{2}(1-e_w^2)\right] \tag{14}$$

On the righthand side of this, the first term represents generation of random particle motion by the diffuse collisions between particles and the wall, while the second term represents dissipation of pseudothermal energy because of the inelasticity of these collisions. (e_w is the coefficient of restitution for particle-wall collisions.) Finally, a boundary condition for the gas velocity at the wall is needed. Though the point value of this variable certainly vanishes everywhere on the wall (and consequently an ensemble average will also vanish there), we are interested in a local average, taken over a spatial region which is large compared with the particle size, and this will not vanish at the wall. The structure of the suspension immediately adjacent to the wall would be expected to differ from that of the bulk and a complete theory of suspension flow should predict this, but for the present purpose we would like to subsume these complexities, in some way, in a boundary condition. Any such proposed condition should degenerate into the no-slip condition at the limit of small particle concentration, and should mandate a very small normal gradient of velocity at the opposite limit of high concentration. An attempt to formulate a boundary condition of this sort was made by Sinclair and Jackson (1989); though neither the derivation nor the final result is entirely satisfactory, it will be retained for the present work in the following form:

$$\left[\beta(\nu)(u_x - v_x) + \frac{\partial p}{\partial x}\right]\delta(\nu) + \mu_{eg}\mathbf{n}\cdot\nabla u_x + \frac{2\mu_{eg}Tu_x}{v_i^2\delta(\nu)} = 0 \tag{15}$$

Here $\delta(\nu) = \delta_o\nu/\nu_o$, where δ_o is a parameter with the dimensions of length which is of the order of size of the spatial averaging region.

The above equations and boundary conditions are reduced to dimensionless form by introducing the following scaled variables:

$$y^* = \frac{y}{H}; \quad u^* = \frac{u}{v_t}; \quad v^* = \frac{v}{v_t}; \quad T^* = \frac{v}{v_t^2}; \quad p^* = \frac{p}{\rho_p Hg} \tag{16}$$

then, after introducing the closure relations for the stress, the drag force, and the pseudothermal energy flux, Eqs. 1-4 become:

$$\frac{\partial}{\partial y^*}\left(\mu^*_{eg}(\nu)\frac{\partial u^*}{\partial y^*}\right) - \frac{Re}{F}\left[\frac{\nu(u^*-v^*)}{(1-\nu)^2} + \frac{\partial p^*}{\partial x^*}\right] = 0 \tag{17}$$

$$\frac{\nu}{F}\left[\frac{(u^*-v^*)}{(1-\nu)^2}-\sin\theta\right]+d^*\frac{\partial}{\partial y}\left(\sqrt{T^*}\,\mu^* f_1(\nu)\frac{\partial v^*}{\partial y^*}\right)+\sin\phi\,\mathrm{sgn}\left(\frac{\partial v^*}{\partial y^*}\right)\frac{\partial N_f^*}{\partial y^*}=0 \quad (18)$$

$$\frac{\partial}{\partial y^*}\left[f_2(\nu)T^*+N_f^*\right]+A\nu=0 \quad (19)$$

$$\frac{\partial}{\partial y^*}\left(\lambda^*\sqrt{T^*}\,f_3(\nu)\frac{\partial T^*}{\partial y^*}\right)+\mu^*\sqrt{T^*}f_1(\nu)\left(\frac{\partial v^*}{\partial y^*}\right)^2-f_5(\nu)\frac{T^{*3/2}}{d^*}=0 \quad (20)$$

The boundary condition (Eq. 13), applied at each wall, gives:

$$\frac{\partial v^*}{\partial y^*}=\frac{\phi' f_8(\nu)v^*}{d^*}-\frac{N_f^*}{d^*\sqrt{T^*}\mu^* f_1(\nu)}\times\left[\sin\phi\,\mathrm{sgn}\left(\frac{\partial v^*}{\partial y^*}\right)-\mathrm{sgn}\,(v^*)\tan\delta\right] \quad \text{at} \quad y^*=0 \quad (21)$$

and

$$\frac{\partial v^*}{\partial y^*}=-\frac{\phi' f_8(\nu)v^*}{d^*}-\frac{N_f^*}{d^*\sqrt{T^*}\mu^* f_1(\nu)}\times\left[\sin\phi\,\mathrm{sgn}\left(\frac{\partial v^*}{\partial y^*}\right)+\mathrm{sgn}\,(v^*)\tan\delta\right] \quad \text{at} \quad y^*=1 \quad (22)$$

while the "pseudothermal" boundary condition (Eq. 14) similarly gives:

$$\frac{\partial T^*}{\partial y^*}-(1-e_w^2)\frac{f_9(\nu)}{d^*}T^*+\frac{\phi' f_{10}(\nu)v^*}{d^*}+\frac{f_4(\nu)}{f_3(\nu)}T^*\frac{\partial \nu}{\partial y^*}=0 \quad \text{at} \quad y^*=0 \quad (23)$$

and

$$-\frac{\partial T^*}{\partial y^*}-(1-e_w^2)\frac{f_9(\nu)}{d^*}T^*+\frac{\phi' f_{10}(\nu)v^*}{d^*}-\frac{f_4(\nu)}{f_3(\nu)}T^*\frac{\partial \nu}{\partial y^*}=0 \quad \text{at} \quad y^*=1 \quad (24)$$

Finally, the gas-phase boundary condition (Eq. 15) gives:

$$\frac{Re\,\delta^* f_6(\nu)}{F\mu_{eg}^* f_7(\nu)}\left[\frac{\nu}{(1-\nu)^2}+\frac{\partial p^*}{\partial x^*}\right]+\frac{\partial u^*}{\partial y^*}+\frac{T^* u^*}{\delta^* f_7(\nu)}=0 \quad \text{at} \quad y^*=0 \quad (25)$$

and

$$\frac{Re\,\delta^* f_6(\nu)}{F\mu_{eg}^* f_7(\nu)}\left[\frac{\nu}{(1-\nu)^2}+\frac{\partial p^*}{\partial x^*}\right]-\frac{\partial u^*}{\partial y^*}+\frac{T^* u^*}{\delta^* f_7(\nu)}=0 \quad \text{at} \quad y^*=1 \quad (26)$$

In these equations, we have introduced several dimensionless variables and parameters, defined as follows:

$$x^*=\frac{x}{H};\quad d^*=\frac{d}{H};\quad A=\frac{Hg\cos\theta}{v_t^2};\quad \mu_{eg}^*=\frac{\mu_{eg}}{\mu_g}$$

$$\mu^*=\frac{\mu}{\rho_p d\sqrt{T}};\quad \lambda^*=\frac{\lambda}{\rho_p d\sqrt{T}};\quad N_f^*=\frac{\sigma_{yy}^f}{\rho_p v_t^2}$$

$$F=\frac{v_t^2}{gH};\quad Re=\frac{\rho_p H v_t}{\mu_g} \quad (27)$$

where d is the particle diameter. The dimensionless functions $f_1(\nu)-f_{10}(\nu)$ are defined in Table 1.

The closure relations (Eqs. 13 and 14) were actually modified for small values of the particle concentration to allow for the fact that the mean free path between collisions becomes comparable with the width of the duct. Details of this are given by Sinclair and Jackson (1989) and will not be repeated here.

Table 1. Definition of Dimensionless Functions of $f_1(\nu)-f_{10}(\nu)$

$$f_1(\nu)=\frac{1-\frac{\nu^{1/3}}{\nu_0^{1/3}}+\frac{8}{5}\eta\nu+\frac{8}{5}\eta(3\eta-2)\nu+\frac{64}{25}\eta^2(3\eta-2)\nu^2 g_0(\nu)}{\eta(2-\eta)}+\frac{768\nu^2\eta g_0(\nu)}{25\pi}$$

$$f_2(\nu)=\nu[1+4\eta\nu g_0(\nu)]$$

$$f_3(\nu)=\frac{8}{\eta(41-33\eta)}\left[1-\frac{\nu^{1/3}}{\nu_0^{1/3}}+\frac{12}{5}\eta\nu+\frac{12}{5}\eta^2(4\eta-3)\nu+\frac{144}{25}\eta^3(4\eta-3)\nu^2 g_0(\nu)+\frac{64(41-33\eta)\eta^2\nu^2 g_0(\nu)}{25\pi}\right]$$

$$f_4(\nu)=\frac{8}{\eta(41-33\eta)}\left\{\left[\frac{1}{\nu g_0(\nu)}+\frac{12}{5}\eta\right]\frac{12}{5}\eta(2\eta-1)(\eta-1)\frac{\partial[\nu^2 g_0(\nu)]}{\nu}\right\}$$

$$f_5(\nu)=\frac{48}{\sqrt{\pi}}\eta(\eta-1)\nu^2 g_0(\nu)$$

$$f_6(\nu)=\frac{\nu^2}{2\nu_0^2}$$

$$f_7(\nu)=\frac{\nu}{2\nu_0}$$

$$f_8(\nu)=\frac{\pi}{\mu^*(\nu)f_1(\nu)2\sqrt{3}\left(\frac{\nu_0}{\nu}-\frac{\nu_0^{2/3}}{\nu^{2/3}}\right)}$$

$$f_9(\nu)=\frac{\sqrt{3}\pi}{\lambda^*(\nu)f_3(\nu)4\left(\frac{\nu_0}{\nu}-\frac{\nu_0^{2/3}}{\nu^{2/3}}\right)}$$

$$f_{10}(\nu)=\frac{\pi}{\lambda^*(\nu)f_3(\nu)2\sqrt{3}\left(\frac{\nu_0}{\nu}-\frac{\nu_0^{2/3}}{\nu^{2/3}}\right)}$$

The above equations were solved numerically using orthogonal collocation. For much of the work Lagrange polynomials were used as the basis functions, but in some circumstances (in particular, low gas flow rates at high solids loading in horizontal ducts) these were replaced by Hermite cubic splines. The maximum number of collocation points needed was 48.

The problem contains ten parameters, namely Re, F, d^*, e_p, e_w, δ^*, δ', ϕ, ϕ', and θ; for each set of values of these, the gas pressure gradient and the profiles of solids fraction and velocities must be determined as functions of the flow rates of the two phases. A complete exploration of this is clearly out of the question, and the investigation therefore focuses on one particular set of physical parameters, listed in Table 2, which correspond to the system previously studied by Sinclair and Jackson. The solutions are then examined over the plane of the two flow rates, for three different orientations of the duct, namely vertical, horizontal, and inclined at 45°.

Results and Discussion

Following Sinclair and Jackson (1989), the results of the computations can be summarized by plotting contours of constant pressure gradient, $\partial p/\partial x$, in the plane of the flow rates of the two phases. Dimensionless variables are used, and the flow rates are expressed as dimensionless superficial velocities, defined as follows:

$$Q_s^* = Q_s/Hv_t; \quad Q_g^* = Q_g/Hv_t$$

where Q_s and Q_g are the volume flow rates of solids and gas, respectively, per unit width of the duct perpendicular to the (x, y)-plane.

Figure 2 shows the results of a few calculations for a vertical duct, for comparison with the results of Sinclair and Jackson, which were obtained in a duct of circular cross section. The general picture is not altered by the change from circular to rectangular section, nor by the inclusion of the frictional contribution to the stress. Even the remarkable fine structure, found in the second quadrant by Sinclair and Jackson, is reproduced in the present results, though it is not visible on the scale at which Figure 2 is plotted. The loops in the contours, found by Sinclair and Jackson in the third quadrant, are found in the present results, but it is difficult to follow them when the particle concentration becomes high and the frictional contribution dominates the stress. The condition of symmetry about the center plane of the duct was not imposed in the computations, but the computed velocity and solids concentration profiles were found to be completely symmetric, providing a test of accuracy.

Similar results for a duct inclined at 45° are shown in Figure 3 and, at first glance, they resemble closely the results for the vertical duct. However, a closer examination of the second quadrant would reveal that the fine structure, referred to by Sinclair and Jackson as the "crossback region," is now absent. This is not surprising, as the crossback region is associated with the existence of a solution representing a classical, stationary fluidized bed, and this can exist only in an exactly vertical duct. Figure 4 shows a single contour, corresponding to a dimensionless pressure gradient $dp^*/dx^* = -0.104$, and identifies three points on it. The velocity and solids fraction profiles at these points are then exhibited in Figures 5, 6, and 7. Point 1 corresponds to cocurrent upflow, and the velocity profiles in Figure 5 reveal that each phase is moving upward everywhere in the section. These profiles look almost sym-

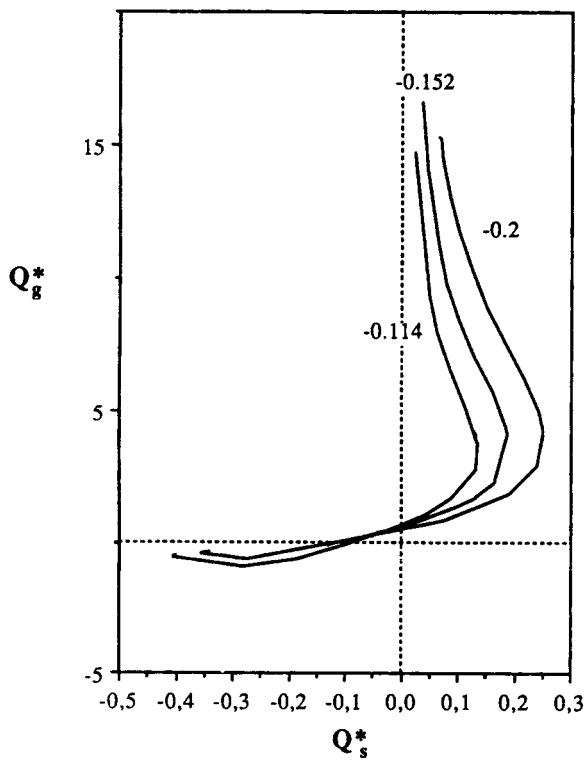

Figure 2. Three contours for $\theta = 90°$.

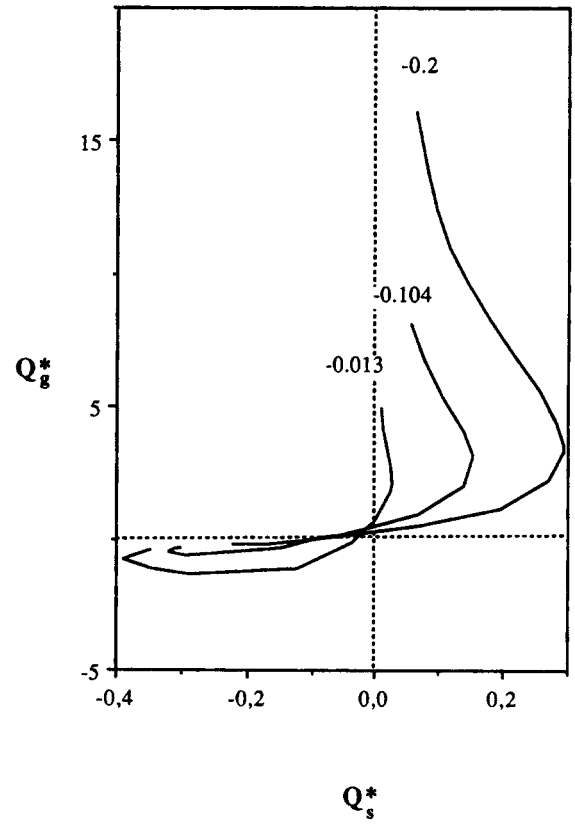

Figure 3. Three contours for $\theta = 45°$.

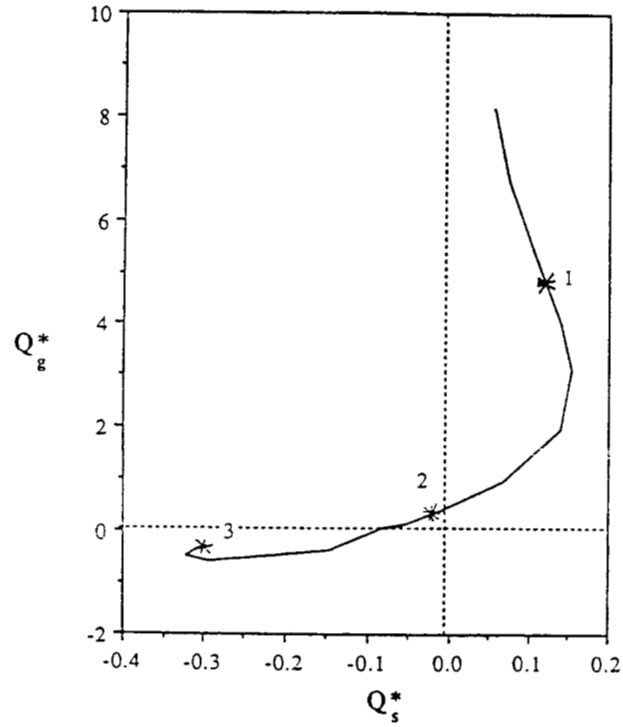

Figure 4. Contour for $dp^*/dx^* = -0.104$ with three identified points.

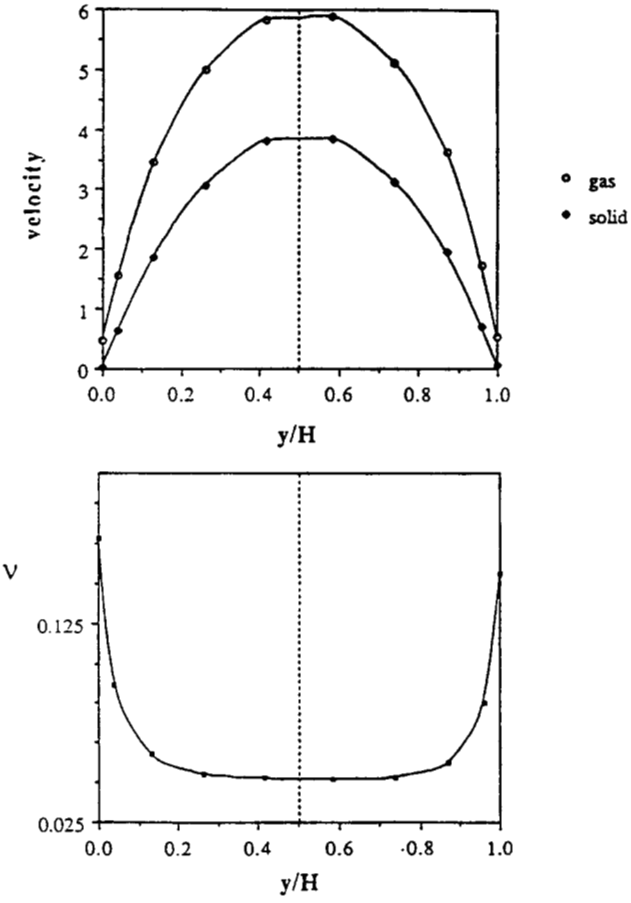

Figure 5. Gas and solid velocities, and volume fraction profiles for point 1, Figure 4.

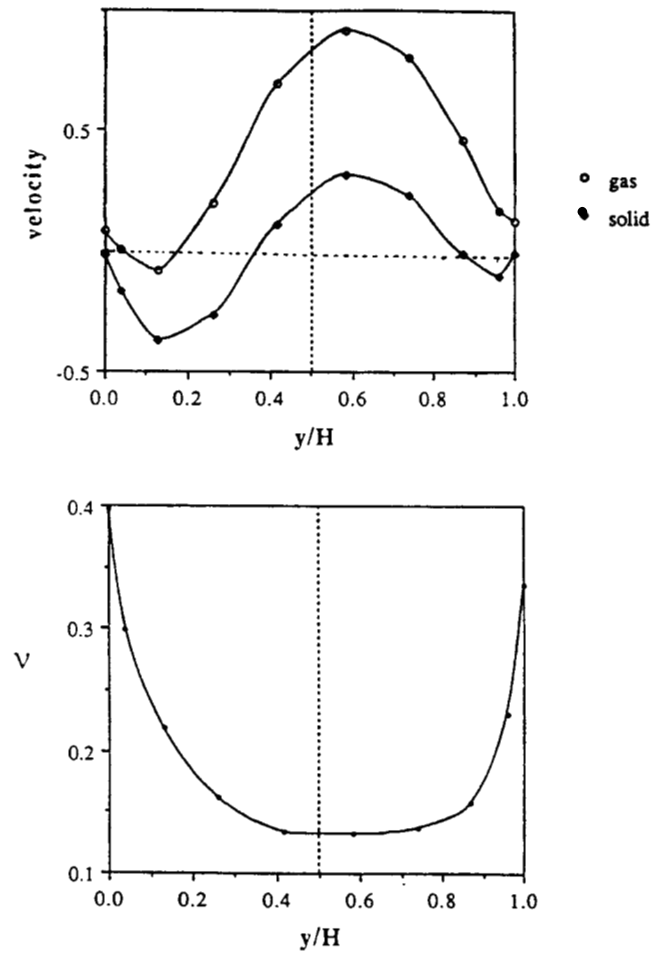

Figure 6. Gas and solid velocities, and volume fraction profiles for point 2, Figure 4.

metric though there is, in fact, a small asymmetry which is most clearly visible in the solids fraction profile. For point 2, which lies in the second quadrant corresponding to countercurrent flow, the velocity profiles of Figure 6 are quite complicated. Though the overall flows are upward for the gas and downward for the particles, each phase ascends in parts of the cross section and descends in others, and both profiles are markedly asymmetric. The solids fraction profile also shows a marked asymmetry, with higher concentrations of particles in the lower part of the duct, as expected. Finally, Figure 7 shows that both solids and gas flow downward everywhere in the cross section at point 3, and the profiles show relatively little asymmetry.

A contour for a smaller value of the pressure gradient is shown in Figure 8 with two identified points, corresponding to cocurrent upflow and countercurrent flow, respectively. The velocity and solids fraction profiles corresponding to point 1 are shown in Figure 9; comparing this with Figure 5 shows that the asymmetries are decidedly stronger for the smaller pressure gradient. This will be a recurring feature of all the results. The distribution of the particles over the cross section is a result of competition between the effect of collisions induced by the shearing motion, which tend to push the particles out to both walls, and gravitational sedimentation, which tends

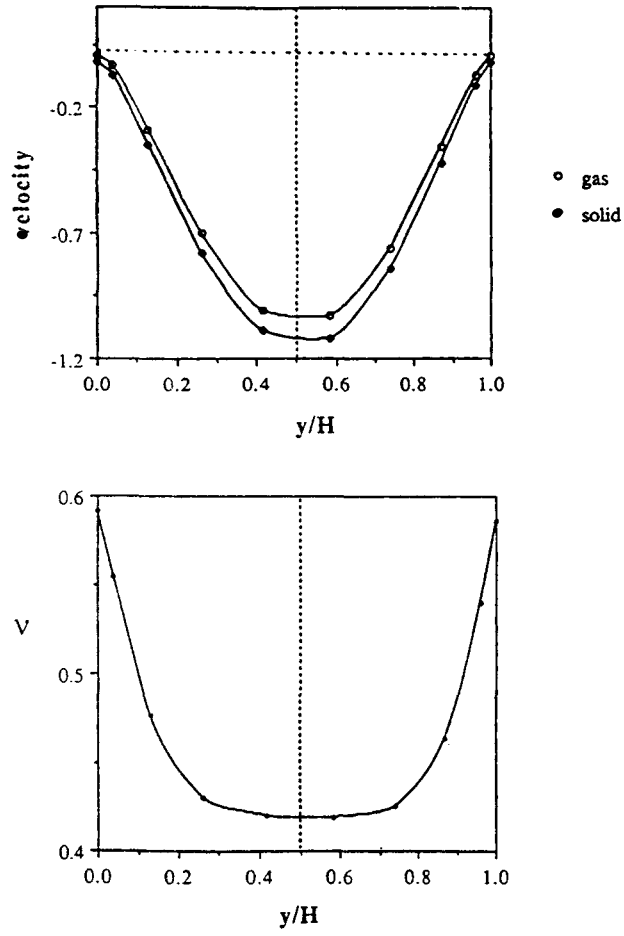

Figure 7. Gas and solid velocities, and volume fraction profiles for point 3, Figure 4.

to pull them down to the lower wall. Under conditions leading to large *frictional* pressure gradients the former effect dominates and the asymmetry is weak, while when the frictional pressure gradient is small gravity induces stronger asymmetries. Figure 10 shows the velocity and volume fraction profiles for point 2, which is just within the region of countercurrent flow. There is now a layer adjacent to the lower wall where the particle concentration is much larger than in the center of the duct and a second, less pronounced increase in concentration near the upper wall. The particles flow downward in the dense layer and drag gas with them, whereas in the upper part of the duct the gas flows upward and drags the particles in that direction. The direction of flow is therefore determined mainly by the gas pressure gradient in the upper part of the duct, but by the axial component of the gravity force in the lower part.

When the duct is horizontal the direction of flow is determined entirely by the gas pressure gradient, so countercurrent flow or flow against this gradient is impossible. Consequently, the contours of constant pressure gradient in the (Q_s^*, Q_g^*) plane are confined to the first quadrant. Figure 11 shows three such contours. Once again, at high values of the pressure gradient, the dispersive effect of collisions between particles is the dominant factor in determining the distribution of the particles over the cross section, and gravitational sedimentation has little effect. This is seen in the velocity and solids fraction profiles of Figure 12, which belong to point A identified on

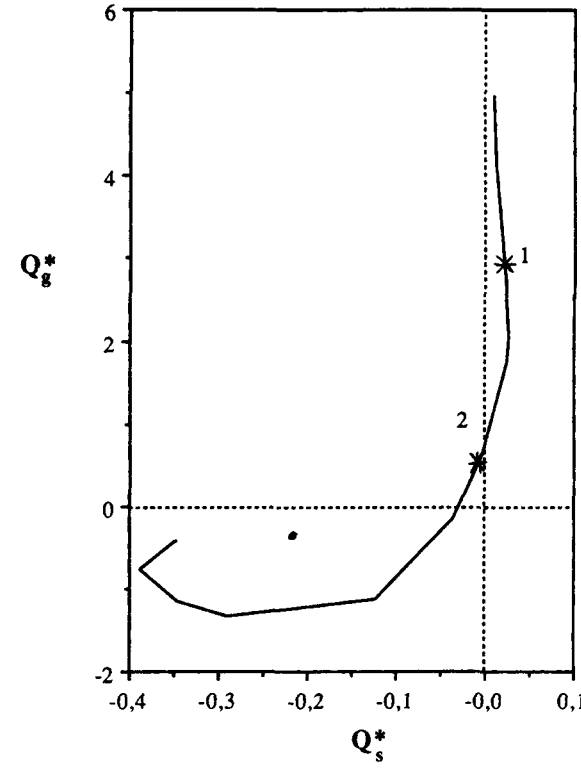

Figure 8. Contour for $dp^*/dx^* = -0.013$ with two identified points.

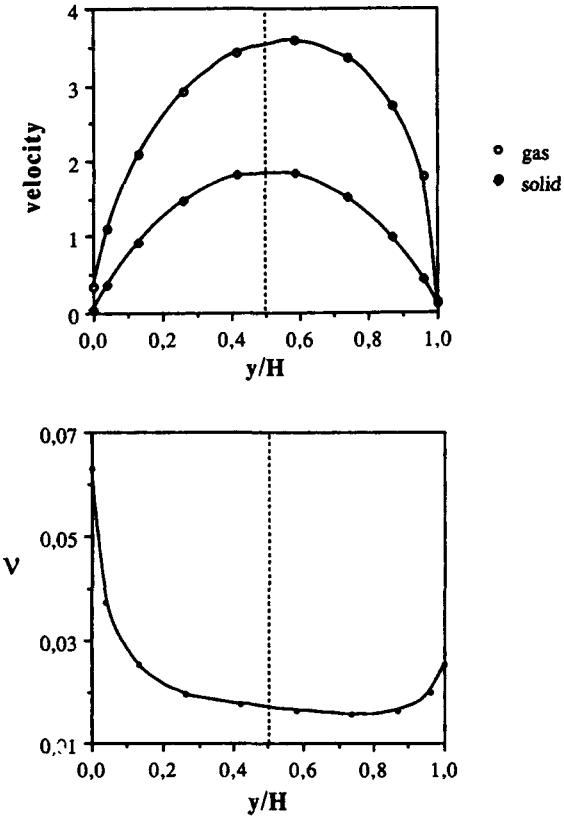

Figure 9. Gas and solid velocities, and volume fraction profiles for point 1, Figure 8.

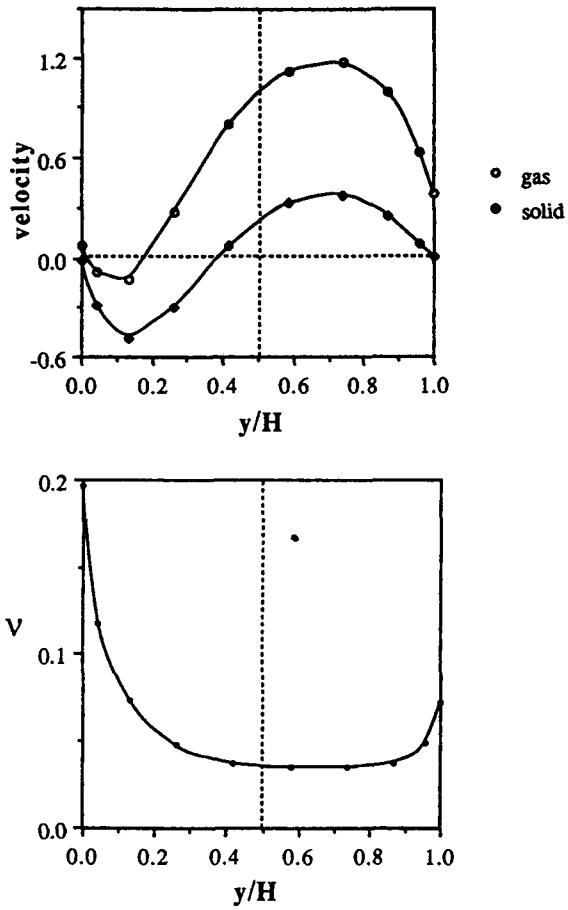

Figure 10. Gas and solid velocities, and volume fraction profiles for point 2, Figure 8.

the contour $dp^*/dx^* = -0.2$ in Figure 11. The profiles are almost symmetric about the center plane. However, when the pressure gradient is reduced by a factor of ten, the gravitational asymmetry becomes apparent. The profiles in Figure 13 correspond to point B, identified on the pressure gradient contour for $dp^*/dx^* = -0.02$ in Figure 11. Although the solids volume fraction now comes quite close to random close packing at the lower wall of the duct, there is still a layer of enhanced concentration adjacent to the upper wall. The pressure gradient must be reduced by another decimal order of magnitude before we see the pattern commonly observed in horizontal pneumatic transport lines, namely a dense layer of particles sliding slowly in contact with the lower wall, propelled by a rapidly moving and relatively dilute suspension occupying the upper part of the duct. The solids fraction profile for such a case is presented in Figure 14, together with the profile of granular temperature. Now there is no increase in particle concentration on approaching the upper wall. The solids fraction in contact with the lower wall is near random close packing, and the granular temperature there is very small. The dense layer does not have a sharp upper surface; instead, the solids fraction decreases continuously and the granular temperature increases on moving up, with the upper half of the duct occupied by a suspension which nowhere contains more than about 3% solids by volume. Figure 15 shows the corresponding velocity profiles for both solids and gas. There is a thin layer adjacent to the lower wall, which is moving slowly in plug flow. Above this, the velocities

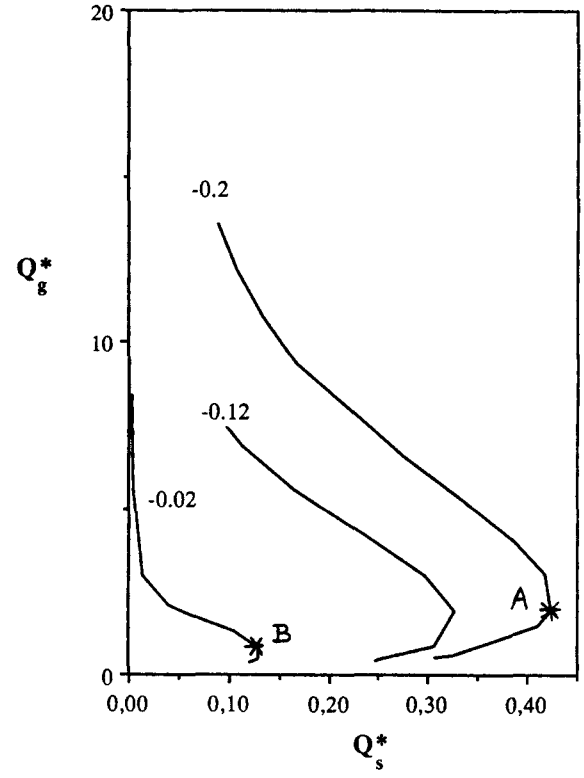

Figure 11. Three contours for $\theta = 0°$.

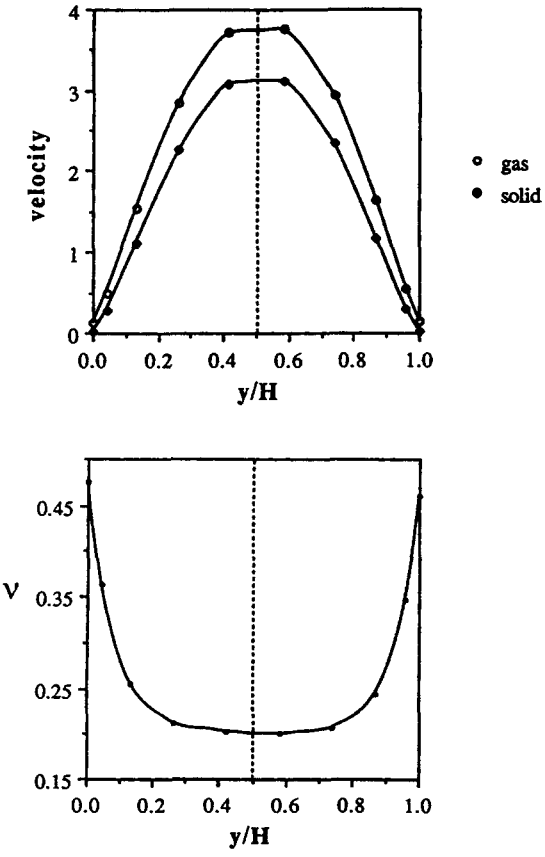

Figure 12. Gas and solid velocities, and volume fraction profiles for point A, Figure 11.

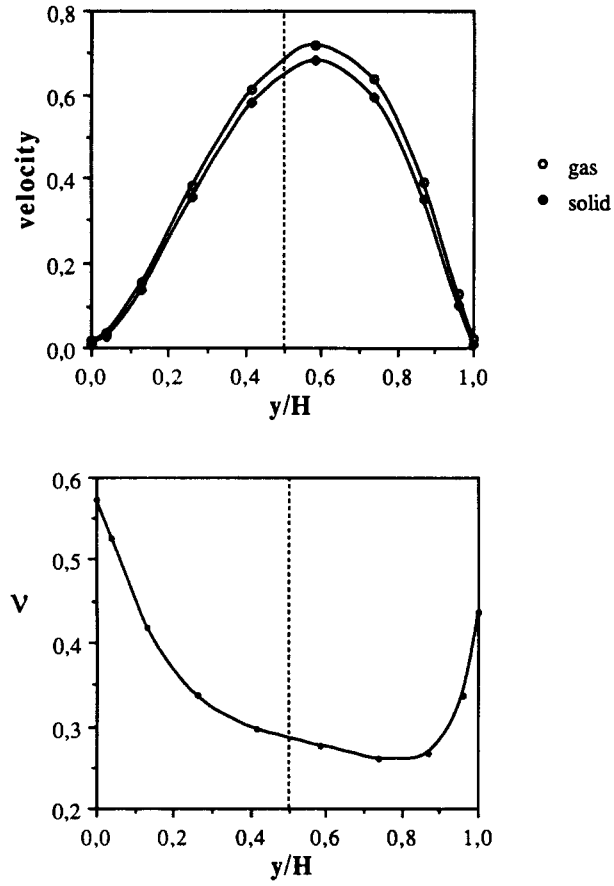

Figure 13. Gas and solid velocities, and volume fraction profiles for point B, Figure 11.

of both phases increase, but the slip remains quite small until about the mid plane, after which it increases rapidly in the part of the duct which can be regarded as containing a flowing suspension.

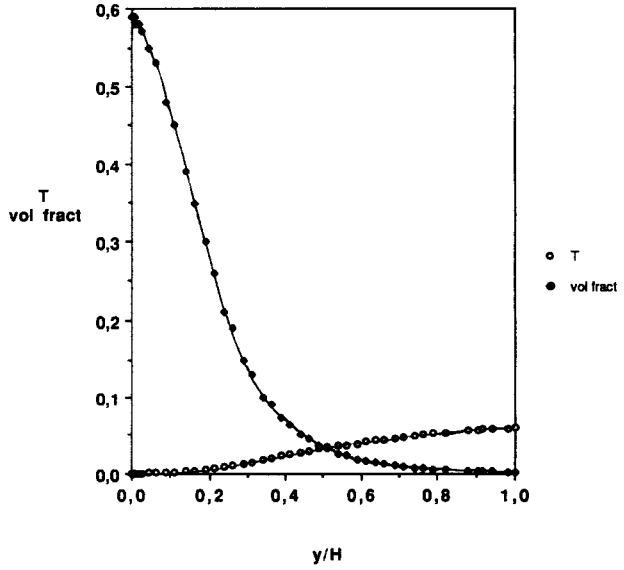

Figure 14. Profiles of volume fraction and particle temperature, $Q_s^* = 0.0106$, $Q_g^* = 0.36$.

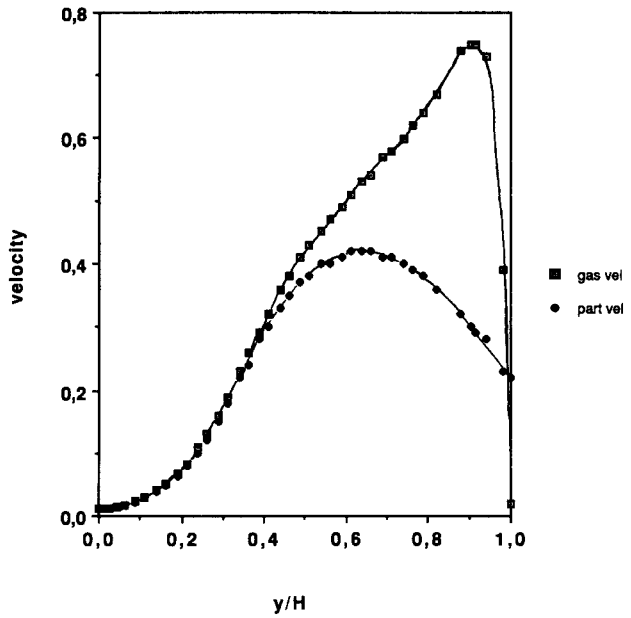

Figure 15. Profiles of gas and particle velocities, $Q_s^* = 0.0106$, $Q_g^* = 0.36$.

It is not surprising that, for comparable degrees of symmetry in the computed profiles, the pressure gradient is smaller in the horizontal duct than in the duct inclined at 45°. In the latter case, the weight of the particles transported by the gas is a major contributor to the total pressure gradient, so for the same value of the frictional contribution (and hence the same dispersion by collisions) the total pressure gradient needs to be larger.

The results seem to model quite well the expected variations in physical behavior with flow rates and duct inclination. However, they are very sensitive to the value of the coefficient of restitution for collisions between particles. If this is reduced only slightly from unity, the tendency of the particles to subside as a dense layer on the lower surface of a horizontal duct is greatly increased. This can be seen in Figure 16, where conditions are similar to those of Figure 14, except that η is reduced from unity to 0.998. The dense layer is now thicker than that of Figure 14, and the transition from this layer to the flowing suspension above occurs much more sharply. To emphasize the dramatic effect of small changes in the coefficient of restitution the solids fraction profile immediately adjacent to the lower wall is plotted in Figure 17 for $\eta = 1$, 0.999 and 0.998, other conditions remaining unaltered. This great sensitivity of the results to the value of the coefficient of restitution was also noted by Sinclair and Jackson (1989), while Pita and Sundaresan (1991) found that inclusion of damping of the pseudo-thermal motion by the gas-particle drag force had a similar effect to a reduction in the coefficient of restitution.

Finally, it is interesting to explore the effect of the duct width on the results. All the results so far presented are for the conditions of Table 2, which specifies a duct width of 3 cm. A limited number of computations was also made for ducts of different widths to explore the sort of problems that might be expected in scaling. Some results are shown in Figure 18, where the dimensionless pressure gradient dp^*/dx^* [$= (dp/dx)/\rho_p g$] is plotted, as a function of the (dimensional) duct

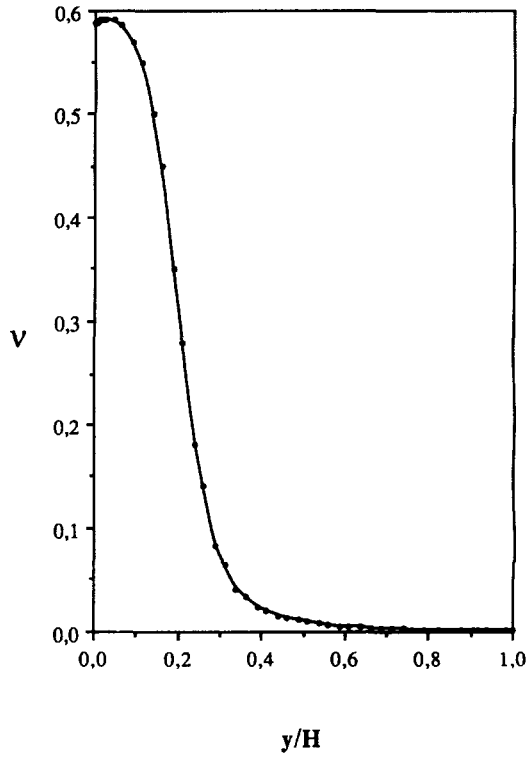

Figure 16. Particle concentration profile, $dp^*/dx^* = -0.0014$, $\eta = 0.998$.

width, for vertical ducts with given values of the gas and particle fluxes, namely $Q_g^* = 5$ and $Q_s^* = 0.1$. For small values of the width the pressure gradient decreases rapidly as the width increases, while for large widths there is a slow increase in the pressure gradient with width. Between the two extremes there

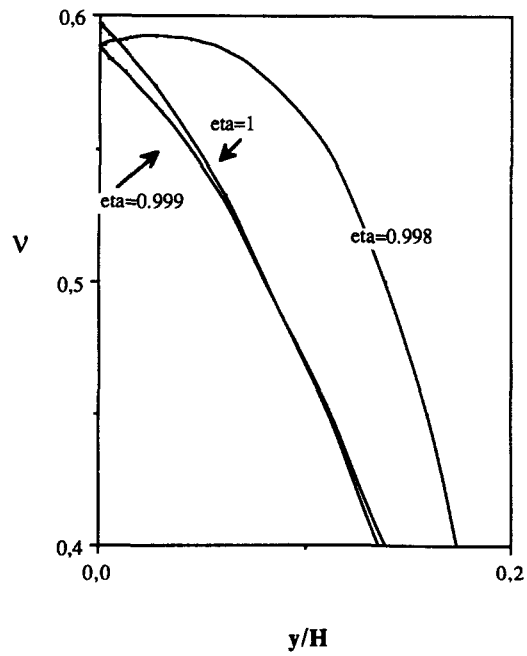

Figure 17. Particle concentration profiles for different values of η.

Table 2. Parameters Used in the Simulation

d	Particle diameter	0.00015 m
ρ_p	Particle density	2,500 kg/m^3
H	Duct's width	0.030 m
μ_g	Gas viscosity	0.0365 cp
v_t	Particle terminal velocity	1.29 m/s
e_p	Particle-particle coefficient of restitution	1.0
e_w	Particle-wall coefficient of restitution	0.9
ϕ'	Specularity coefficient	0.5
ν_0	Maximum allowed solid volume fraction	0.65
ν_m	Critical solid volume fraction	0.5
Fr	Parameter in Eq. 11	0.05 N/m^2
n_1	Parameter in Eq. 11	2
p	parameter in Eq. 11	3
δ'	Wall angle of friction	15°
n	Parameter in Eq. 5	2
δ_0	Boundary layer thickness	0.00075 m
ϕ	Angle of internal friction	28°

appears to be an interval of multiple states. This is sketched as a broken line, since we did not attempt to follow the contour through the branch points. These findings are consistent with published results of Pita and Sundaresan (1991). There are indications that even more complicated behavior may be found in certain circumstances, so it is doubtful that scale-up can be successful without a sound theoretical basis.

Conclusions

The collective effects which result from collisions between particles in a flowing suspension, which were shown by Sinclair and Jackson (1989) to generate much of the characteristically complex behavior observed in vertical ducts, have been shown here to account for many features of flow in inclined and horizontal ducts. This is perhaps surprising, since the theory treats only laminar flow, while in most situations of technical importance the motion might be expected to be vigorously turbulent. Quantitatively useful prediction should not, therefore, be expected, and this is underlined by the extreme sen-

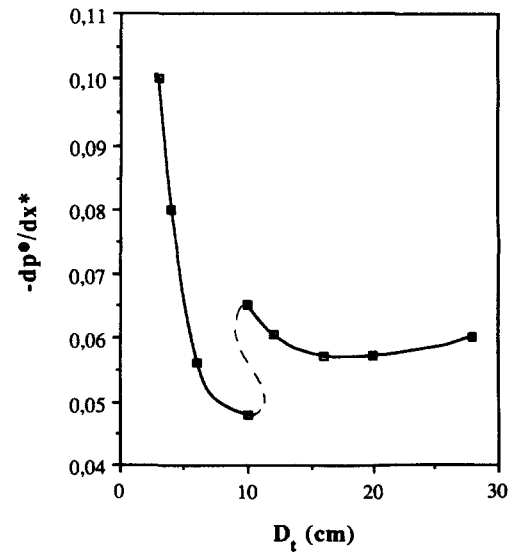

Figure 18. Axial pressure gradient vs. duct width.

sitivity of the results to particle properties such as the coefficient of restitution. Though direction experimental information on this is not available, one suspects that it is not nearly such an important factor in practice. This is not surprising if the flows of practical interest are turbulent, since momentum transfer associated with the turbulent fluctuations will then be a factor, and it may dominate the kinetic-collisional and frictional mechanisms treated in the present work.

It is clear, then, that an extension of the work to model turbulent flow is imperative if quantitative results are to be obtained for technically important flows. A start in this direction has been made by Louge et al. (1991), who confined attention to the case of massive particles which do not follow turbulent fluctuations in the gas velocity. Tsuo and Gidaspow (1990) have also solved numerically the full time-dependent equations of motion for the interacting gas and particles, and their solutions for flow in a vertical duct exhibit velocity fluctuations and inhomogeneities in particle concentration on a scale comparable with the duct diameter. Nevertheless, the theory of laminar flow, developed in this article and the earlier work of Sinclair and Jackson, is not without value any more than the Poiseuille solution for single-phase flow. In particular, the laminar solutions have demonstrated the importance of contact interactions in endowing the assembly of particles with a collective behavior of its own, so that it should be regarded as a second phase in interaction with, but not merely passively responsive to, the motion of the gas. In particular, this has important implications for the treatment of turbulent flow of gaseous suspensions of solid particles. In the past the particles have been treated as an inert burden, responding to the turbulent fluctuations in the gas velocity and hence tending to damp these fluctuations. When collisional interactions between the particles are important, the shearing of the particle phase itself might be expected to generate instabilities that contribute to the turbulent fluctuations, so it is no longer clear where the energy source for the turbulence resides.

Acknowledgment

This work has been supported by the International Fine Particle Research Institute and, in its earlier stages, by the National Science Foundation under Grant No. CBT-8504201.

Notation

A = particle diameter
e_p, e_w = particle-particle and particle-wall coefficients of restitution
H = lateral dimension of duct
I = dissipation rate due to inelastic collisions
m = particle mass
p = local average gas pressure
q_{pT} = axial pseudothermal energy flux
Q_s, Q_g = volume flow rates of solids and gas per unit duct width
T = particle temperature
u = local average axial gas velocity
v = local average axial solids velocity
v_t = terminal fall velocity of isolated particle in air
x, y = Cartesian coordinates (see Figure 1)

Greek letters

β = drag coefficient for gas-particle force
δ' = angle of friction between particles and wall
θ = inclination of duct to the horizontal
μ_g, μ_{eg} = viscosity and effective viscosity for gas phase
ν = solids volume fraction
ρ_p = density of solid material
σ_{ij} = components of particle phase stress tensor
$\sigma_{ij}^c, \sigma_{ij}^p$ = "collisional" and "frictional" parts of σ_{ij}
ϕ = angle of friction for particle assembly
ϕ' = specularity factor for particle-wall collisions

Literature Cited

Campbell, C., "Rapid Granular Flows," *Ann. Rev. Fluid Mech.*, **22**, 57 (1990).

Jackson, R., "Some Mathematical and Physical Aspects of Continuum Models for the Motion of Granular Materials," *Multiphase Flow*, p. 291, Academic Press (1983).

Jenkins, J. T., "Rapid Shear Flows of Granular Materials," *Non-Classical Continuum Mechanics: Abstract Techniques and Applications*, R. J. Knops and A. A. Lacey, eds., Cambridge University Press (1987).

Johnson, P. C., and R. Jackson, "Frictional-Collisional Constitutive Relations for Granular Materials, with Application to Plane Shearing," *J. Fluid Mech.*, **176**, 67 (1987).

Johnson, P. C., P. Nott, and R. Jackson, "Frictional-Collisional Equations of Motion for Particulate Flows and Their Application to Chutes," *J. Fluid Mech.*, **210**, 501 (1990).

Louge, M. Y., E. Mastorakos, and J. T. Jenkins, "The Role of Particle Collisions in Pneumatic Transport," *J. Fluid Mech.*, **231**, 345 (1991).

Lun, C. K. K., S. B. Savage, D. J. Jeffrey, and N. Chepurniy, "Kinetic Theories for Granular Flow: Inelastic Particles in Couette Flow and Slightly Inelastic Particles in a General Flow Field," *J. Fluid Mech.*, **140**, 223 (1984).

Pita, J. A., and S. Sundaresan, "Gas-Solid Flow in Vertical Tubes," *AIChE J.*, **37**, 1009 (1991).

Richardson, J., and W. Zaki, "Sedimentation and Fluidization: I," *Trans. Instn. Chem. Engrs.*, **32**, 35 (1954).

Savage, S. B., "Granular Flows Down Rough Inclines—Review and Extension," *Proc. of U.S.-Japan Seminar on New Models and Constitutive Relations in the Mechanics of Granular Materials*, J. T. Jenkins and M. Satake, eds., Elsevier (1982).

Sinclair, J. L., and R. Jackson, "Gas-Particle Flow in a Vertical Pipe with Particle-Particle Interactions," *AIChE J.*, **35**, 1473 (1989).

Tsuo, Y. P., and D. Gidaspow, "Computation of Flow Patterns in Circulating Fluidized Beds," *AIChE J.*, **36**, 885 (1990).

Manuscript received Oct. 23, 1992, and revision received Jan. 22, 1993.